UDC 550.42 Geochemistry International, 30(11), 1993

Mineralogical and Geochemical Features of the Manus Basin Hydrothermal Sulfide Ores, Bismarck Sea*

A.Yu. Lein, N.V. Ul'yanova, V.A. Grinenko, Ye.V. Bibikova, and A.P. Lisitsyn

Vernadskiy Institute of Geochemistry and Analytical Chemistry,
Russian Academy of Sciences, Moscow

Paragenetic mineral assemblages have been established based on mineralogical, chemical, and isotope (S, Pb) studies, and the sequence of deposition has been defined in hydrothermal sulfide structures in a typical back-arc basin. The ores in the Manus basin have a prominent Zn specialization (sphalerite, würtzite, and fe-sphalerite). An association of Fe-sphalerite and galena with Ag sulfosalts is noted that is not characteristic of typical midocean ridge hydrothermal systems. The average ^{34}S in the sulfide minerals is 3.5‰, which corresponds to the medium-temperature sphalerite stage in hydrothermal mineral formation. It is suggested that the metal source is located in the relatively acid rocks of the island-arc tholeiitic series and possibly in sediments.

The Manus Basin is a typical back-arc basin. Hydrothermal activity in the rift system there has been known since 1985 [1]. The ore shows in the basin were first examined in May–June 1990 [2, 3].

We have examined the mineral and geochemical features of hydrothermal sulfide ores in a series of midocean ridge rift systems [4–7]. The purposes of this study were to identify the specific features of hydrothermal mineralization in back-arc basin rifts and compare them with mineralization in open-ocean rift systems.

Materials and Methods

The material was collected in May 1990 on the 21st voyage of the R/V *Academician Mstislav Keldysh* by means of *Mir-1* and *Mir-2* manned submersibles [3].

The hydrothermal ores were examined by traditional optical microscopy: immersion analysis and the examination of thin sections and polished sections in transmitted and reflected light.

We used a Camscan scanning electron microscope with Link AN-10000 energy-dispersive analyzer at an accelerating voltage of 15 kV to examine the morphology and provide a preliminary identification of the mineral phases.

A Camebax Microbeam probe was used at 20 kV, 30 nA, and probe diameter 1.5–2.5 μm to determine the compositions of the minerals. The standards were certified synthetic and natural compounds. The standard ZAF correction procedure was applied. We eliminated any analysis whose sum did not fall in the range 100 ± 3%.

---

* Translated from Geokhimiya, No. 4, pp. 524–537, 1993.

ISSN0016-7029/93/0011-0057

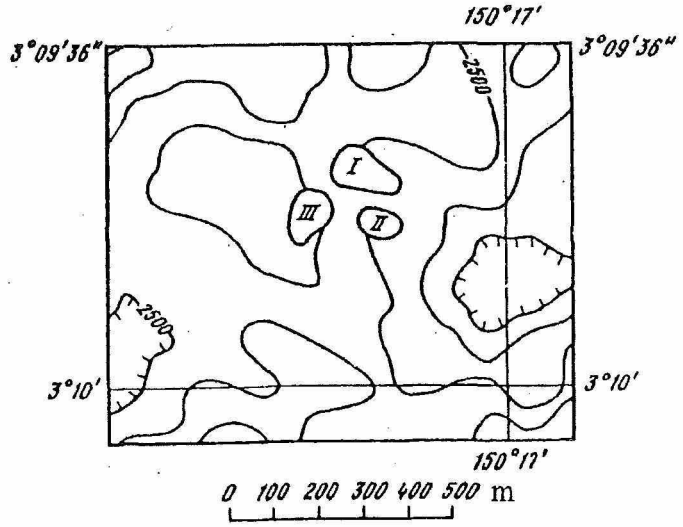

Fig. 1. Disposition of the hydrothermal fields in the Manus polygon, station 2255, *Mir* submersible (L.P. Zonenshayn): I) Vienna Woods active field (specimens 2255-2 to 14); II) White Tower active field (specimens 2255-15 and 16); III) hydrothermal sulfide structures (inactive field), *Dead Wood* (specimen 2255-17).

Mineral samples (or their assemblages if the grain size was fine) were taken for sulfur isotope analysis after detailed mineralogical and petrographic description and the identification of the paragenetic assemblages.

the Pb isotope compositions were determined on samples of sulfide and sulfate minerals selected by hand, which were dissolved in a mixture of HNO_3 and HCl. The lead was isolated chromatographically with Dowex AG 1 × 8 anion exchanger [8].

The lead isotope compositions were measured with a Cameca TSN-206A mass spectrometer by thermionic emission using silica gel as the ion emitter. The isotope ratios were normalized to the NBS-981 lead standard. The isotope ratios were measured with an accuracy of ±0.1%.

We used an MI-1305 instrument at this institute with the [9] method in the isotope analyses of the sulfur in the hydrothermal products.

Geological Setting and Mineral and Chemical Compositions of the Hydrothermal Products

Our specimens (Table 1) were taken from three hydrothermal fields within the Red Star dome in the inner rift (Fig. 1) at depths of 2500–2505 m. The hydrothermal products from the Vienna Woods field were examined in the most detail (Table 1 and Fig. 1). A geological description has been given along with the characteristics of the structures in this region in [1–3], so we will give only a brief description of the sampling locality (Table 1).

Two main structural elements were detected from the Mir (aquanaut L.P. Zonenshayn) in the Vienna Woods: a "base," which consisted of sheet-type mineralized crusts and young pillow basalt lavas with sulfide mineralization in the form of crusts (specimens 2255-13 and 14), and tubular structures on the base with heights up to 14 m. These included active ones (specimens 2255-2 and 10) and extinct ones (specimen 2255-4). The maximum temperature of the hydrothermal fluid from the tube where specimen 2255-11 was taken was 275.7°C [3].

The Manus Basin ores have prominent zinc specialization. The zinc sulfides are sphalerite and würtzite. There are smaller amounts of pyrite and marcasite and even less of chalcopyrite,

Table 1

Brief Characteristics of Station M-2255 Specimens

Sampling point	Spec. No.	Minerals		
		main (>25%)	minor (25–5%)	rare (<5%)
Vienna Woods hydrothermal field, 3°09.75' S, 150°16.83' E				
Base deposits: sulfide crusts on basalts with distinct banded textures	5	Sphalerite, würtzite	Pyrite, marcasite, chalcopyrite	Galena, Al silicate
	7	Pyrite, marcasite	Sphalerite, chalcopyrite, barite, silica	Galena, anglesite, Cu sulfide
	13	Sphalerite, würtzite	Pyrite, marcasite, chalcopyrite, barite	Silica
	14	Sphalerite, pyrite	Silica	Chalcopyrite, galena, Cu sulfide, Ag sulfosalts
Small tubes intergrown	6	Barite	Würtzite, pyrite, marcasite	Na chloride, silica
Small structures at edge of field:				
active	2	Sphalerite, würtzite, pyrite	Silica, barite	Chalcopyrite, galena, anhydrite
inactive	4	Barite, silica	Sphalerite, pyrite, marcasite, würtzite	Galena, anglesite, Cu sulfides
Large tubular structures, active (gray smokers):				
top of active tube	11	Sphalerite, anhydrite	Fe-sphalerite	—
wall of active tube	10	Sphalerite, würtzite, barite	Pyrite, marcasite	Chalcopyrite, anglesite, silica
fragment of structure (from scree)	9	Pyrite, marcasite, barite	Sphalerite, cristobalite	Chalcopyrite, galena, anglesite
White Tower hydrothermal field, 3°09.8'S, 150°16.85'E				
Tops of active hydrothermal structures	15	Silica	Barite, sphalerite, würtzite, chalcopyrite, anhydrite	Galena, Mg-silicate
Dead Wood hydrothermal field				
Top of inactive hydrothermal structures	17	Sphalerite, würtzite	—	Chalcopyrite, pyrite, marcasite

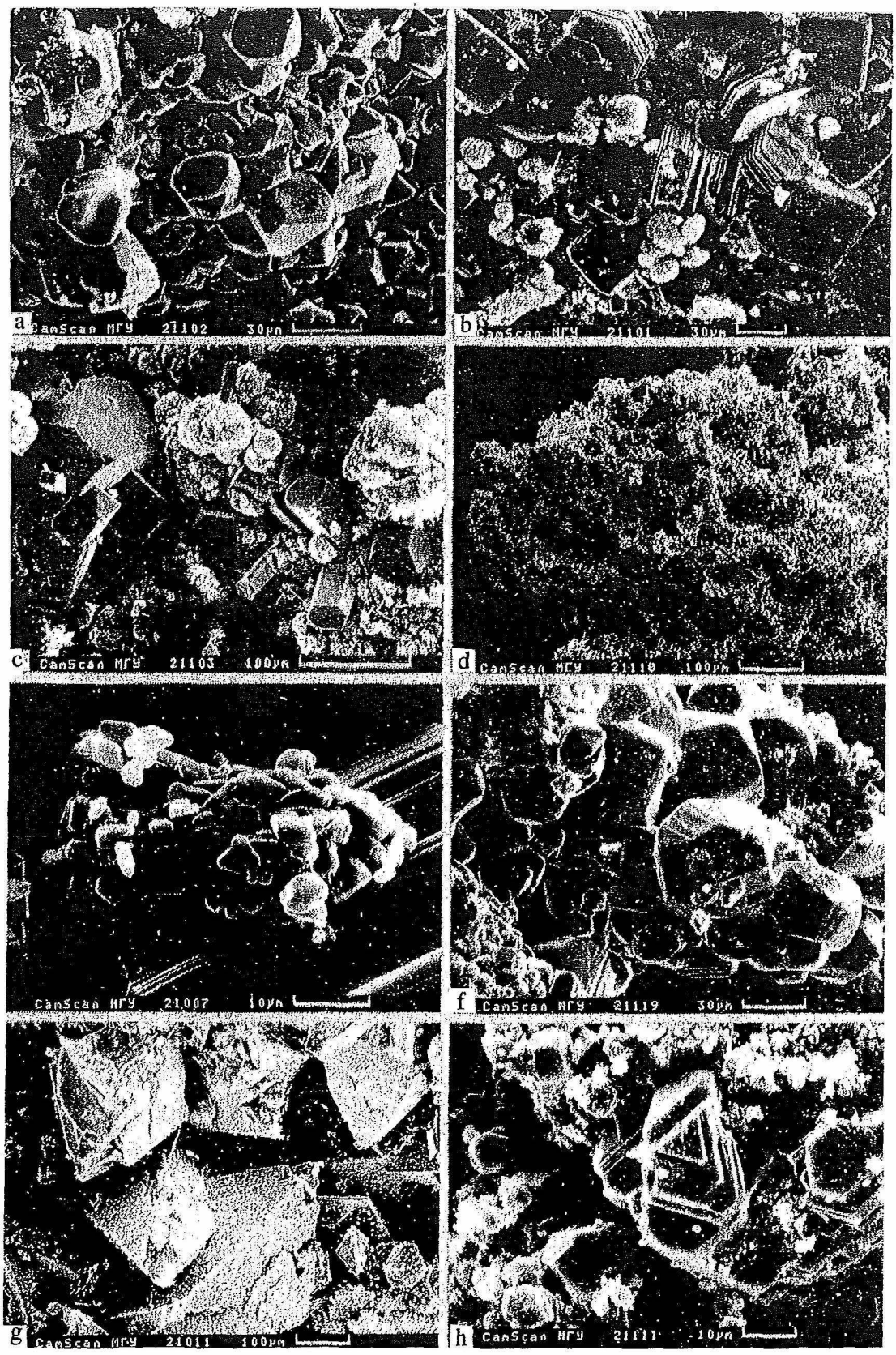

Fig. 2. Morphology of and relationship between minerals and Manus hydrothermal constructions. Polymetallic ores: a) sphalerite ores (main stage, specimen 14); b) tabular (micaceous) würtzite crystals, cubic pyrite crystals, and droplet-like silica aggregates in sphalerite ore (specimen 14); c) hexagonal würtzite prisms, pyrite crystals of cube-octahedron habit, and droplet silica from geodes (specimen 14); d) porous sphalerite ore with pumice-like texture (specimen 13); e) crystals of anhydrite and ferroan sphalerite on hexagonal tabular würtzite crystal (specimen 11); f) pyrite crystals with pentagonal-dodecahedral habit from dark-gray pyrite-sphalerite ore (main stage, specimen 13); g) flocculent type marcasite crystals from geodes (specimen 9); h) tetrahedral-habit

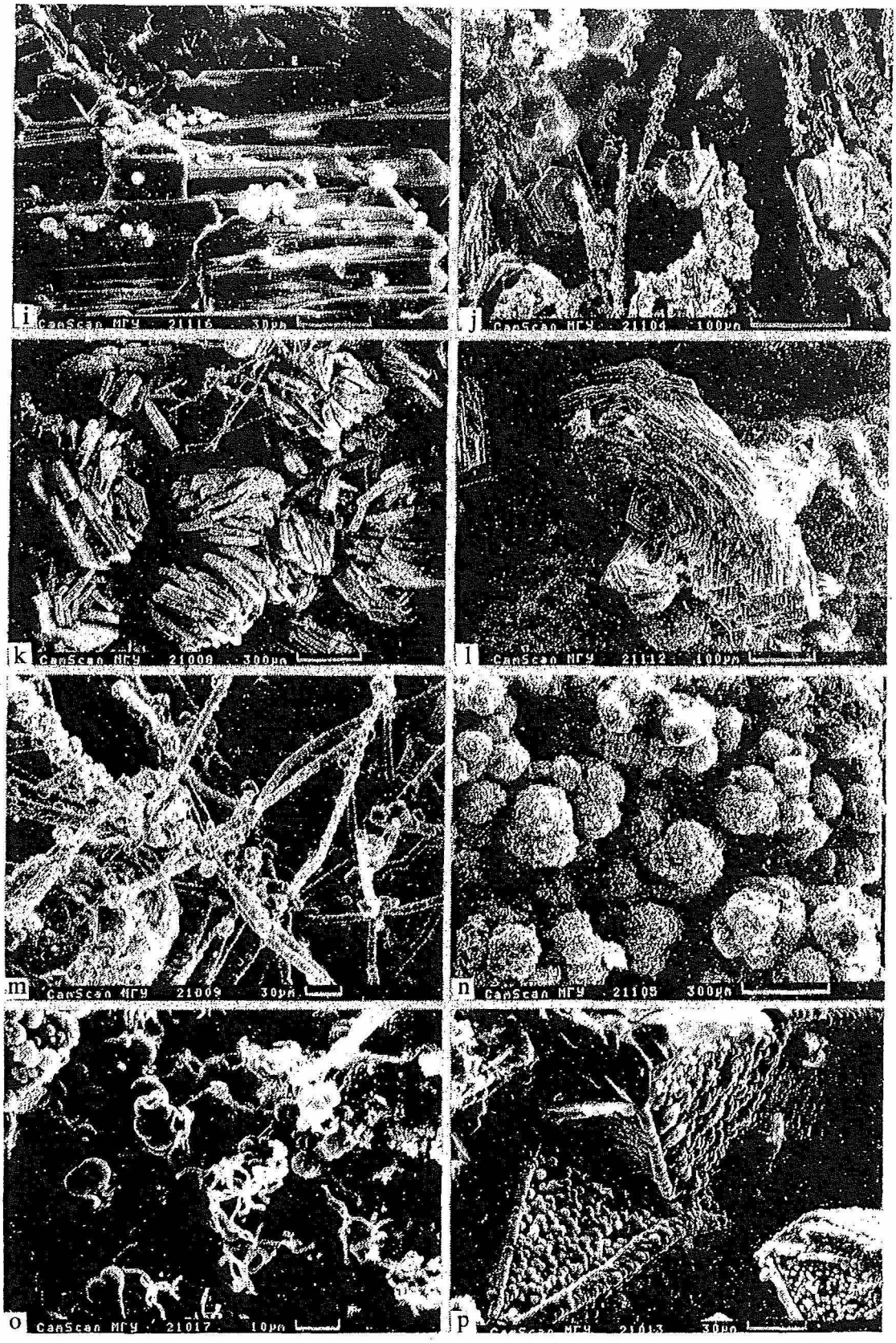

chalcopyrite crystals in sphalerite-würtzite ore (specimen 17); nonore rock components: i) anhydrite with spherical Mg silicates (specimen 15/4); j) acicular polycrystalline copper chloride aggregates (atacamite?) amongst hexagonal würtzite crystals (specimen 14); k) tabular barite crystals (specimen 6); l) rosette-like barite (specimen 4); m) whisker-like deposit of silica in barite matrix (specimen 6), fragment in Fig. 3); n) globular silica aggregate containing very small (1–3 μm) sulfide crystals (specimen 2); o) SiO_2 globules and Fe-Si bearing products resembling bacterial cells in morphology (specimen 6); p) silica jacket on marcasite crystals (specimen 9).

Table 2 (part I)

Mineral, parameter	Spec. No.	S	Pb	Cd	Fe	Zn	Cu	Mn	Bi	Ag	Sb	As	Co	Ni	Σ
ZnS	5(19)	32,87	0,11	0,34	2,32	63,82	0,36	0,02	0,07	0,01	0,54	0,01	0,01	0,01	100,43
std		1,43	0,05	0,16	1,26	2,09	0,37								
k		1	0,001	0,003	0,040	0,954	0,005	0,000							1,003
ZnS	7(5)	33,65	0,34	0,10	8,73	56,18	0,69	Not obs.	0,01	0,04	0,43	0,04	0,00	0,01	100,21
std		0,30	0,28	0,04	1,73	2,27	0,39								
k		1	0,002	0,001	0,149	0,819	0,010	"							0,981
ZnS	14(20)	33,10	1,74	0,03	4,39	59,47	0,51	0,05	0,13	0,51	0,59	0,15	0,01	0,01	100,64
std		1,92	1,57	0,03	1,71	1,73	0,25								
k		1	0,008	0,000	0,075	0,884	0,008	0,000							0,976
FeS_2	5(4)	53,32	0,13		43,47	2,06	0,17	0,26	0,17	0,15	0,33	0,17	0,02	0,01	100,24
std		0,54	0,17		0,92	2,02	0,08	0,15							
k		2	0,001		0,936	0,038	0,003	0,006							0,984
Pyrite	5(2)	52,95	0,22		42,89	3,81	0,22	0,34							100,43
k		2	0,001		0,930	0,071	0,004	0,007							1,014
Marcasite	5(2)	53,69	0,03		44,04	0,31	0,12	0,18							98,37
k		2	0,000		0,942	0,006	0,002	0,004							0,954
FeS_2	7(7)	53,72	0,02		45,42	0,03	0,02	0,04	0,19	0,06	0,26	0,05	0,03	0,01	99,87
std		0,35	0,03		1,03	0,02	0,02	0,08							
k		2	0,000		0,971	0,001	0,000	0,001							0,973
Pyrite	7(3)	53,67	0		46,08	0,05	0,04	0,08							99,92
k		2	0		0,986	0,001	0,001	0,002							0,989
Marcasite	7(4)	53,76	0,04		44,93	0,03	0,01	0,01							98,78
k		2	0,000		0,960	0,000	0,000	0,000							0,961
FeS_2	14(11)	53,15	0,17	0,02	45,65	0,32	0,05	0,15	0,32	0,03	0,05	0,04	0,03	0,01	99,94
std		1,40	0,10		0,78	0,37	0,04	0,11							
k		2	0,001	0,000	0,987	0,006	0,001	0,003							0,998

Pyrite	14(4)	53,00	0,12	0,04	46,03	0,39	0,05	0,12						99,69
k		2	0,001	0,000	0,998	0,007	0,001	0,003						1,009
Marcasite	14(5)	53,91	0,22		45,16	0,31	0,07	0,17						99,84
k		2	0,001		0,962	0,006	0,001	0,004						0,974
$CuFeS_2$	5(3)	35,46	0,17		27,77	2,13	33,26	0,00	0,11	0,06	0,40	0,01	0,02	0,01	99,39
std		0,32	0,15		0,59	0,56	0,37	0,00							
k		2	0,001		0,899	0,059	0,947	0,000							1,906
$CuFeS_2$	7(4)	35,35	0,11		28,59	1,19	33,43	0,01	0,10	0,01	0,28	0,25	0,02	0,01	99,36
std		0,45	0,08		0,76	0,24	0,66	0,01							
k		2	0,001		0,956	0,007	0,959	0,001							1,923
$CuFeS_2$	14(7)	35,88	0,14		29,30	1,46	33,13	0,01	0,16	0,20	0,07	0,02	0,02	0,01	100,40
std		0,32	0,11		0,52	0,74	0,32	0,02							
k		2	0,001		0,938	0,040	0,932	0,000							1,911
PbS	7(3)	14,40	85,96	0,03	1,57	0,11	0,05								102,12
std		0,42	0,92	0,04	1,05	0,07	0,03								
k		1	0,924	0,001	0,004	0,053	0,002								0,984

Note: *Std*, variance; *k*, coefficient in crystallochemical formula; numbers in parentheses, numbers of analyses. Analyst K.I. Ignatenko, this institute.

Table 2 (part II)

Mean Chemical Composition and Crystallochemical Formulas of Barite

Mineral, parameter	Spec. No.	BaO	CaO	PbO	SrO	SiO_2	SO_3	Σ
$BaSO_4$	7(2)	63,08	0,31	0,03	2,36	0,17	33,49	99,43
$BaSO_4$	14(5)	62,78	0,15	0,16	1,24	0,67	33,10	98,10
std		1,77	0,11	0,19	1,50	1,08	0,54	

Note: *Std*, variance of contents; *k*, coefficient in crystallochemical formula; numbers in parentheses, numbers of analyses. Analyst K.I. Ignatenko, this institute.

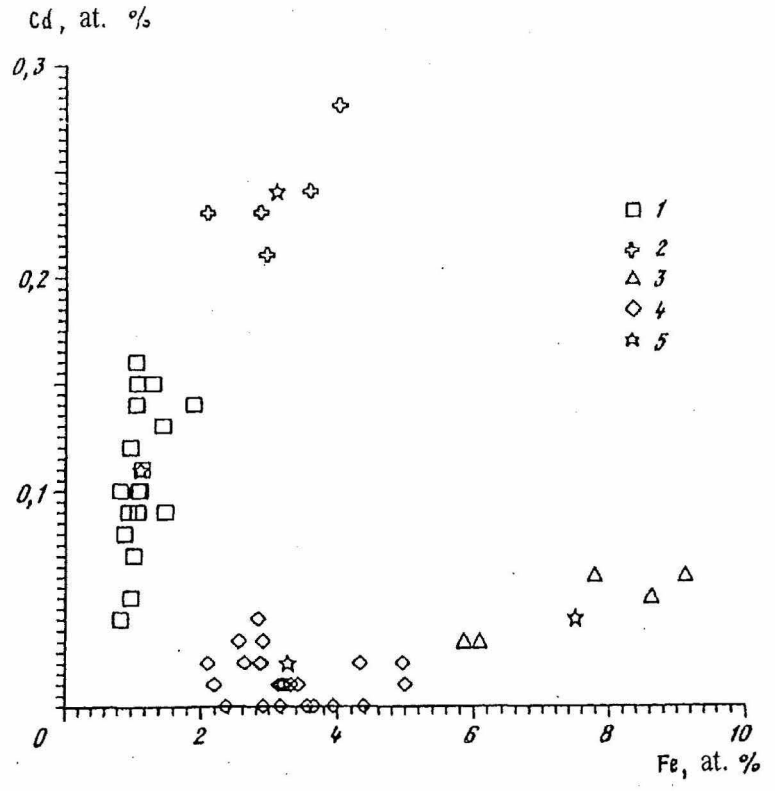

Fig. 3. Variations in Cd and Fe contents of sulfides: 1) sphalerite, specimen 2255-5; 2) würtzite, specimen 2255-5; 3) sphalerite, specimen 2255-7; 4) sphalerite, specimen 2255-14; 5) mean value of analysis in group.

while occasionally one finds galena and copper sulfides (Table 1). Of the gangue minerals, barite and silica minerals (opal and cristobalite) predominate, and occasionally anhydrite. There are small amounts of anglesite and copper chlorides (atacamite?) and sodium chloride, together with Mg, Ca, and Al silicates and silver sulfosalts.

The Zn sulfides frequently form crystals of tetrahedral habit (sphalerite) or hexagonal tablets and short prisms (würtzite, Fig. 2, a–c)). The sizes of the microcrystals range from 2–5 up to 50–100 μm. ZnS micrograins also participate in the kidney-shaped sulfide-opal aggregates (Fig. 2c) and in the pumice-like products (Fig. 2d). The main minor elements in the Zn sulfides are Fe (2–11 wt. %), Cd (0.1 wt. %), Cu (up to 1%), and Pb (up to 5%) (Table 2). High concentrations of the last are not characteristic of the Zn polymorphs and occurred only in specimen 14, where there are also Bi, Ag, Sb, and As at a level of tenths of a percent. The elevated Cd in würtzite by comparison with sphalerite is due to the preferential entry of the hexagonal greenockite minal CdS into the hexagonal würtzite. The sphalerite and würtzite segregations are not spatially separated and frequently occur within a single specimen (Fig. 2e, specimen 11). As a rule, the tabular and hexagonal prismatic würtzite crystals fill numerous cavities, while the sphalerite crystals are more characteristic of the main ore mass.

The Zn sulfides clearly differ in their formation temperatures in the Cd-Fe diagram (Fig. 3). The low-temperature sphalerites (specimen 14), including the high-iron varieties (specimen 7), do not contain more than 0.065% Cd. The higher-temperature sphalerites and particularly the würtzites (specimen 5) contain on average 0.24% Cd.

Fe disulfides characteristically accompany the sulfide-sulfate mineralization. They form joint aggregates with the zinc sulfides and also form rims 1–10 mm thick around geodes filled with ZnS crystals. The iron sulfides vary in morphology. Pyrite usually forms crystals of pentagonal-dodecahedron habit, with prominent striations on the faces, and with cubic forms rarer (Fig. 2 b–d). Marcasite forms drusy aggregates and flocculent crystals, sometimes in silica jackets (Fig. 2g, p). The composition of the pyrite is almost constant, while the marcasites show minor deviations from stoichiometry (Table 2). The trace-element contents usually do not exceed tenths of a percent.

Chalcopyrite is a minor phase. Its grains are associated with cavities and pores (Fig. 2e), but sometimes it forms emulsion inclusions in sphalerite. The microprobe showed that the chalcopyrites from the crusts on the basalts contain up to 2.7% Zn, while the other trace elements constitute not more than 0.7%. The amounts of Bi, Ag, Sb, and As range from 0.01 to 0.1%, while Co and Ni are in the range 0.01–0.03%. There are variations in the Sb, As, and Ag contents in the chalcopyrites from different areas.

Galena is frequently present in the interstices between the main ore-forming phases and itself forms micrograins of size <0.05 mm, while it is also present as emulsion inclusions in sphalerite. The galena is of constant composition. There are up to 2% of iron and from 0.0 to 0.1% Zn and Cu. A correlation is observed of Ag with Sb + As ($R > 0.65$), which may indicate that there are microscopic inclusions of Ag-bearing sulfosalts. This correlation is clearer in specimen 14 from the crust on basalt. Ag and Pb sulfosalts have previously been found in hydrothermal rocks from the Guaymas depression [4]. Specimens 7 and 4 contain isolated crystals of copper sulfide, while specimen 14 contains copper chloride of atacamite type (Fig. 2j).

Barite is the main gangue mineral and forms sulfide-barite and sulfide-barite-opal assemblages. It occurs as microgranular masses, compound rosette-like and drusy aggregates, and euhedral tabular and prismatic crystals (Fig. 2, k and l). It contains up to 2.5% strontium.

Anhydrite is the main gangue mineral in specimens 11 and 15 from high tubular structures. It forms massive granular aggregates or occurs as platy crystals in association with hexagonal ZnS (Fig. 2i).

Silica may make up the crests of the hydrothermal structures as the main mineral there (specimens 4 and 15), but in sulfide assemblages it is usually present in small amounts (Table 1). The forms are very varied: irregular shapeless particles, reniform and drusy aggregates, and intricate whisker formations consisting of closely spaced spheres (Fig. 2, m–p).

Anglesite forms transparent crystals up to 2 mm in size (specimen 9). In specimen 7, the microprobe detected a phase corresponding in composition to $PbSO_4$, which contains ~0.1% Fe and 0.01% Zn and Cu.

Mg, Ca, and Al silicates occur as isolated grains in specimens from the tubular structures. The tall structures contain minute spheres of magnesium silicate on the faces of anhydrite (Fig. 2g). In a specimen from the edge of the orefield, there are aluminosilicate spheres on sphalerite and strange coral-type products containing Fe and Si (Fig. 2o).

Paragenetic Mineral Assemblages and Deposition Sequence

We found [6] that we can distinguish mineral formation stages in the very complicated but genetically single hydrothermal process on the basis that it evolves and leads to the near-simultaneous or even synchronous formation of mineral assemblages separated in space and

differing in composition. Even naked-eye description of the hydrothermal structures in the Manus Basin shows clearly that there is zonation in the deposition in the sulfide crusts on the base and in the tubular structures. The tube walls grow simultaneously on the inside and outside, which also complicates distinguishing the mineral formation sequence.

To some extent, there are three main stages in the hydrothermal mineralization here, which differ in mineral sets, chemical composition, and morphology; there are also mineral assemblages characteristic of the supergene stage.

Mineral formation stages in the Vienna Woods hydrothermal field

Early:	
low-temperature (up to 170°C) and medium-temperature (up to 270°C)	Barite + pyrite (marcasite) + silica + sphalerite
Main ore formation: (>270°C)	Sphalerite (würtzite) + pyrite + chalcopyrite
Late:	
(<250°C)	Reniform marcasite + Fe-sphalerite + pyrite + silica + galena; galena + Ag sulfosalts + barite + anhydrite + anglesite
Supergene alteration	Fe hydroxides + SiO_2 minerals + atacamite (?) + Mg, Ca, and Al silicates + chlorides + S

In the early stage, paragenetic associations are formed of pyrite (marcasite)-barite or pyrite (marcasite)-opal type. As in the previously researched hydrothermal structures in the open ocean (TAG, Mount Axial), this mineral assemblage is preserved only in some fragments of the structure, e.g., within the intergrown tubes at the edge of the field (specimen 2255-6).

The main stage of ore formation involved the deposition of euhedral sphalerite (würtzite) crystals, iron disulfides, and small amounts of chalcopyrite. Sometimes the assemblage contains silica minerals. Often the granular sphalerite ore contains areas of finely divided sphalerite having a pumice-like texture (Fig. 2d).

A special assemblage is represented by the minerals from geodes (Fig. 2, c and f), which are formed by cooler solutions. This late stage is characterized also by the occurrence of anhydrite and ferroan sphalerite, which developed in crystals of Zn-bearing sulfide minerals from the main stage (Fig. 2e).

That assemblage often contains galena and Ag sulfosalts. A similar assemblage containing ferroan sphalerites (marmatites) has been described previously for the Guaymas hydrothermal structure, where the fluid temperature from microinclusions is 170°C [4, 7]. This late mineral generation is dominated by anhydrite (Fig. 2i), barite (Fig. 2, k and l), and silica minerals (Fig. 2, n–p).

Sulfur-Isotope Composition of Minerals from the Manus Hydrothermal Field Structures

We examined the isotope composition of the sulfur from the main forms of hydrothermal product: sulfide ores making up the active tall structure in the central field of the Vienna Woods and the inactive structure in the Dead Woods field (Table 3). Here we give data on monomineralic

Table 3

Isotope Composition of Sulfide and Sulfate Minerals from Manus Basin Hydrothermal Structures

Spec. No.	Mineral	$\delta^{34}S$, ‰
	Vienna Woods hydrothermal field Sulfide crusts on basalts at edge of field	
5-1	Sphalerite (würtzite) from chalcopyrite-pyrite-sphalerite assemblage	3.2
5-2	Same	3.3
13-1	Sphalerite from sphalerite-pyrite assemblage containing barite and opal	1.3
13-2	Sphalerite (würtzite) from chalcopyrite-pyrite-sphalerite assemblage	2.8
13-3	Pyrite, the same	3.8
13-4	Barite, the same	22.0
13-5	Fe sphalerite from Fe-sphalerite-pyrite-marcasite assemblage	4.0
14-1	Sphalerite from sphalerite-pyrite assemblage containing barite	2.1
14-2	Same	2.3
	Inactive small structure at periphery of field	
4	Fe sphalerite from Fe sphalerite-pyrite-marcasite assemblage containing barite	4.0
	Wall of High Active Tube	
10-1	Sphalerite from sphalerite-pyrite assemblage containing opal and anhydrite	1.9
10-2	Sphalerite from chalcopyrite-pyrite-sphalerite assemblage: a	3.2
	b	3.2
	c	3.0
	d	3.3
10-3	Chalcopyrite, the same	3.3
10-4	Anhydrite, the same	20.7
10-5	Fe sphalerite from Fe sphalerite-marcasite-pyrite assemblage containing barite	3.9
10-6	Pyrite, the same	3.1
10-7	Fe sphalerite from Fe sphalerite-marcasite assemblage in geodes	5.5
9-1	Chalcopyrite from chalcopyrite-pyrite-sphalerite assemblage	2.9
9-2	Crystalline anglesite from cavities, the same	14.7
	Dead Wood hydrothermal field High inactive tube	
17-1	Sphalerite from chalcopyrite-pyrite-sphalerite assemblage: a	3.5
	b	2.9
	c	3.1
	d	3.0
17-2	Chalcopyrite, the same	3.3

Table 3 (continued)

Spec. No.	Mineral	$\delta^{34}S$, ‰
17-3	Pyrite, the same: a	3.7
	b	4.1
	c	4.2
	d	6.0
	Sphalerite from early hydrothermal stage (mean of four samples)	1.9
	Sphalerite from main mineralization stage, mean of nine samples	3.4
	Sphalerite from late hydrothermal stage, mean of four samples	4.5
	Pyrite, mean of six samples	3.1
	Chalcopyrite, mean of three samples	3.2
	Anhydrite, monomineralic samples	20.7
	Barite, monomineralic samples	22.0
	Anglesite, monomineralic samples	14.7

samples of sphalerite (würtzite), pyrite (marcasite), chalcopyrite, anhydrite, barite, and anglesite taken from various parts of the ores on the basis of the assemblages and formation stages.

The sulfide-mineral $\delta^{34}S$ range from 1.3 to 6‰ (Table 3). The isotopically lightest varieties of sphalerite (the main mineral in the ores) occurred in the inner layers of the ore crusts adjoining the basalts (specimens 13-1 and 14-1, 2) and also in the central part of the active tube (specimen 10-1). The sphalerite (würtzite) made up massive and porous-cavernous ores, i.e., was formed during the main stage of mineral formation, and was characterized by stable $\delta^{34}S$ varying from 3.0 to 3.3‰ (Table 3, specimen 10-2a-d). The chalcopyrite and pyrite from the paragenetic associations with sphalerite had the same $\delta^{34}S$ (specimen 10-3, 6) or were somewhat heavier than the sphalerite (specimens 17-2, 3 a–d). Values of $\delta^{34}S$ exceeding 4.0‰ were characteristic of sphalerite and Fe-sphalerite from the paragenetic association with floc-type crystals of marcasite from geodes (Table 3, specimens 13-5 and 10-7), i.e., for zinc sulfides formed in the later stage.

The barite and anhydrite in these Manus hydrothermal formations do not differ in sulfur-isotope composition from sulfate minerals in active hydrothermal fields in the open ocean (Table 3, specimens 13-4 and 10-4). The $\delta^{34}S$ for Pb sulfate (anglesite) were 6–8‰ lighter than the sulfur in the barite and anhydrite (Table 3, specimen 9–2), which may mean that the anglesite was formed from mixtures of hydrothermal fluid and sea water, in which the content of the primary fluid was appreciably higher than in the formation of the other sulfate minerals.

The sulfide-sulfur isotopes for the three main stages in the Manus Basin (Vienna Woods) show a slight increase in heaviness of the sulfur in solution as the hydrothermal system aged. This is indicated by that behavior for pyrite, which becomes heavier from the fluid-conducting channel to the edge of the plates of sphalerite ore (Fig. 4, specimen 17), which represents a horizontal section of the sulfide tube from the central channel, which is partly healed. The sphalerite (würtzite) $\delta^{34}S$ in the same section of the plate of massive ore is almost constant (Fig. 4). The sooty sphalerite from the inner wall of the cavity is clearly later and contains more of the heavy S isotope than does the sphalerite from the main massive ore.

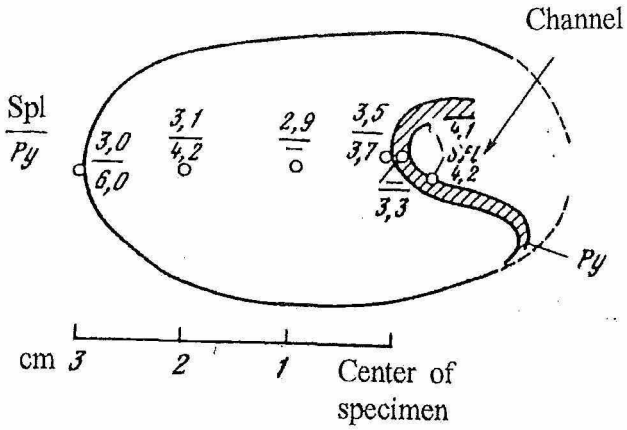

Fig. 4. Variations in isotope composition of sulfur in pyrite Py and sphalerite Spl from the center of the channel to the periphery (plate of thickness 1 cm from tube, specimen 2255/17).

Thus the solutions later than the main mineralization stage contain more ^{34}S and participate in forming the marine sulfate in place of the gradually depleted magmatic sulfur source, which agrees with our earlier data on $\delta^{34}S$ for hydrothermalites in active rifts in midocean ridges [4, 6].

Comparison of data on the sulfur-isotope composition of the sulfide minerals from this rift zone and that for rift zones in midocean ridges indicates the ores with distinct zinc specialization have similar isotope compositions (Fig. 5). The ores with copper specialization are enriched in ^{34}S (Fig. 5, d and e). Pyrrhotite-bearing massive-sulfide ores usually contain more ^{32}S, as is found in the Guaymas Basin ores [4] and in the ores from 21°N in the EPR (Fig. 5a). The evidence can be explained from the dependence of the sulfur isotope fractionation in these ores on the solution temperature. At medium temperatures (170–270°C), which are characteristic of the ores with zinc mineralization in the Juan de Fuca Ridge and Manus Basin, sphalerites are formed with average $\delta^{34}S$ of 3.5‰ (Fig. 5, c and f). If we follow the "geostill" concept, which was at one time popular, island-arc magmatism was decisive in extracting metals from oceanic lithosphere entering subduction zones [10], from which we would expect that the sulfur-isotope composition would be shifted to negative values by comparison with midocean ridge hydrothermalites on account of the isotopically light sulfur from the oceanic lithosphere. Consequently, the Manus sulfur-isotope compositions do not confirm the [10] concept.

Lead isotope analyses [8] show that the Manus ores and the ores in the Lau and West Woodlark Basins have anomalous $^{206}Pb/^{204}Pb$ and $^{207}Pb/^{204}Pb$ by comparison with those in midocean ridges (Fig. 6). The lead isotope data for the hydrothermalites in these three basins fit around the orogen curve in [11], while all known midocean ridge hydrothermalites, apart from the Guaymas Basin ores, i.e. on the mantle curve. Anomalous Pb and Sr isotope compositions occur in southern hemisphere basalts [12, 13], and the causes of these anomalies are related to the origin of the basalts with unusual compositions, which are not considered here. The source of the metals, in particular lead, in back-arc basin hydrothermalites and in midocean ridge hydrothermal ores lies in rocks on the ocean floor with various compositions, which have been involved in the hydrothermal systems.

Conclusions

1. The ores are characterized by distinct Zn specialization and paragenetic assemblages that indicate hydrothermal fluid temperatures of ~270°C.

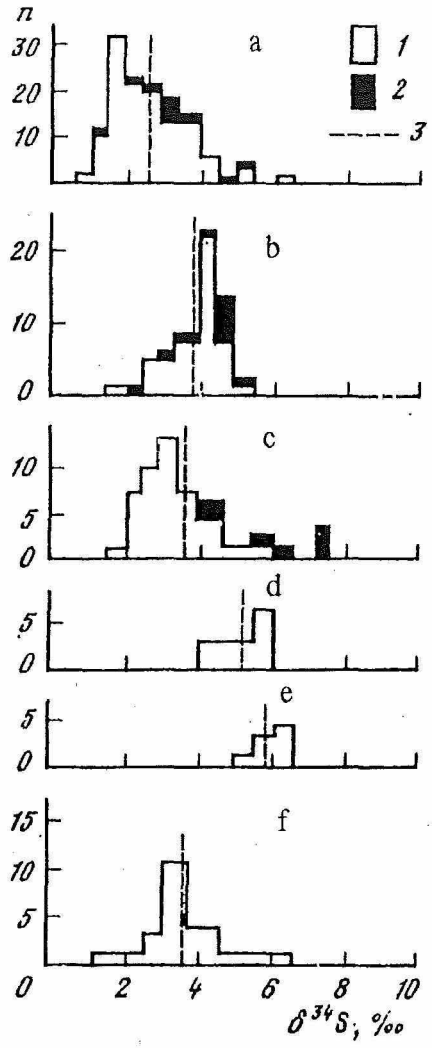

Fig. 5

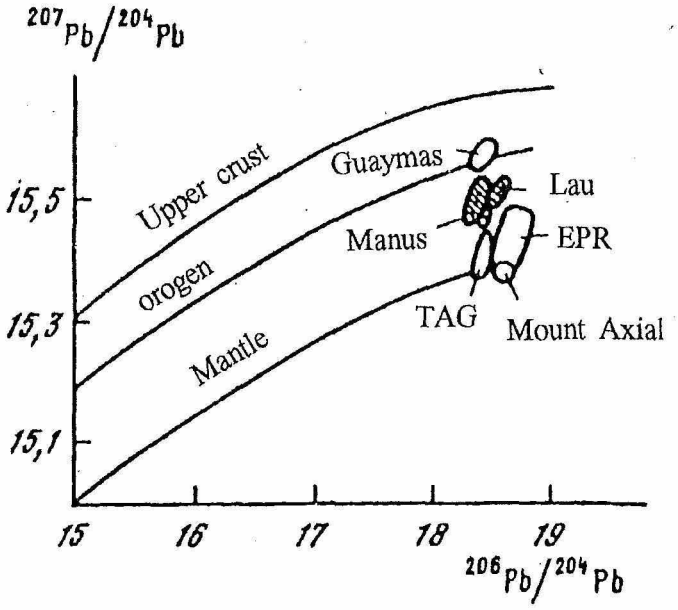

Fig. 6

Fig. 5. Isotope composition of sulfur in sulfides and H_2S from oceanic hydrothermal systems: a) EPR,21° N; b) EPR, 13°N; c) Juan de Fuca Ridge, southern part; d) Mid-Atlantic Ridge, TAG field; e) Galapagos spreading center, 86°W; f) Manus Basin, back-arc spreading area; 1) sulfides; 2) H_2S in solution; 3) mean value, n number of analyses.

Fig. 6. Isotope composition of lead from oceanic-hydrothermal sulfide ores.

2. The association of Fe-sphalerite with galena and Ag sulfosalts is analogous to that previously described [4] for medium-temperature mineral assemblages in geothermal structures in the Guaymas Basin, where sedimentary beds are involved in the formation of the fluid composition.

3. The $\delta^{34}S$ of the main sulfide minerals in the Manus Basin correspond to the medium-temperature sphalerite stage in hydrothermal mineral formation of the type found in the sphalerites in Mount Axial [4] and the southern sector of the Juan de Fuca Ridge [5].

4. The source of the metals for the Manus hydrothermalites is to be seen in magmatites anomalous in Pb and Sr isotopes from the island-arc series, particularly those of acid components.

A specific feature of the hydrothermal mineralization in the Manus back-arc basin is that there is medium-temperature sulfur-bearing galena in association with Fe sphalerite in the ores, whose source may have been sedimentary beds of Guaymas type, which is relatively unlikely, or relatively acid rocks from the island-arc tholeiitic series, or else the two together.

REFERENCES

1. Both, R., K. Crook, B. Taylor, et al., 1986. EOS, AGU, **67**, No. 21, 489.
2. Tufar, W., 1990. Mett. Osterr. Geol. Ges., **82**, 183.
3. Lisitsyn, A.P., K. Kruk, Yu.A. Bogdanov, and L.P. Zonenshayn, 1992. Izv. RAN, Ser. Geol, No. 10.
4. Lein, A.Yu., V.F. Gal'chenko, V.A. Grinenko, et al., 1988. Geokhimiya, No. 9, 1235.
5. Grichuk, D.V. and A.Yu. Lein, 1991. Dokl. AN SSSR, **318**, No. 2, 422.
6. Lein, A.Yu., N.V. Ul'yanova, V.A. Grinenko, and A.P. Lisitsyn, 1991. Geokhimiya, No. 3, 307.
7. Naumov, V.B., O.F. Mironova, V.Yu. Prokof'yev, and A.Yu. Lein, 1991. Geokhimiya, No. 1, 39.
8. Bibikova, E.V., T.V. Gracheva, A.Yu. Lein, and V.A. Makarov, 1991. Second Japan-USSR Symposium on Isotope Geology. Abstracts, Tokyo (Japan), p. 24.
9. Ustinov, V.I. and .V.A. Grinenko, 1965. Pretsizionnyy mass-spektormetricheskiy metod opredeleniya izotopnogo sostava sery [A Precision Mass Spectrometric Method of Determining Sulfur Isotope Compositions], Nauka, Moscow, p. 95.
10. Rona, P., 1973. Sci. Amer., **229**, 85.
11. Doe, B.R. and R.E. Zartman, 1979. Geochemsitry of Hydrothermal Ore Deposits, edited by H. Barnes, John Wiley and Sons, New York.
12. Hart, S.R., 1984. Nature, **309**, No. 28, 753.
13. Gill, J.B., 1984. Earth Planet. Sci. Lett., No. 68, 443.